JOURNAL OF GEOPHYSICAL RESEARCH, VOL. 111, D24208, doi:10.1029/2005JD006300, 2006

Predicting cloud droplet number concentration in Community Atmosphere Model (CAM)-Oslo

Trude Storelvmo,[1] Jon Egill Kristjánsson,[1] Steven J. Ghan,[2] Alf Kirkevåg,[1] Øyvind Seland,[1] and Trond Iversen[1]

Received 31 May 2005; revised 5 March 2006; accepted 12 July 2006; published 22 December 2006.

[1] A new framework for calculating cloud droplet number, including a continuity equation for cloud droplet number concentration, has been developed and implemented in an extended version of the National Center for Atmospheric Research (NCAR) Community Atmosphere Model version 2.0.1 (CAM-2.0.1). The new continuity equation for cloud droplet number concentration consists of a nucleation term and several microphysical sink terms. The nucleation term is calculated on the basis of a parameterization of activation of cloud condensation nuclei (CCN). A subgrid distribution of vertical velocity is used to calculate the range of supersaturations determining the activation within each model grid box. The aerosol types considered in this study are sea salt, sulfate, black carbon, organic carbon, and mineral dust. The horizontal and vertical distributions of sulfate and carbonaceous aerosols are calculated on the basis of AEROCOM (http://nansen.ipsl.jussieu.fr/AEROCOM) sources. Microphysical sink terms for cloud droplets are obtained from a prognostic cloud water scheme, assuming a direct proportionality between loss of cloud water and loss of cloud droplets. On the basis of the framework described above, the cloud droplet number concentration and cloud droplet effective radius are determined. Cloud microphysical and radiative properties compare reasonably well with satellite observations, giving an indication of the soundness of our approach. Our method of fitting the aerosol size distribution with lognormal modes has been evaluated and was found not to introduce systematic errors in our approach. The aerosol indirect effect estimated in the new framework ranges from -0.13 W/m^2 to -0.72 W/m^2, which is significantly smaller than in most other comparable studies. This is largely due to the introduction of microphysical sinks for cloud droplets and a cloud droplet activation scheme which accounts for the so-called competition effect among CCN. As we are not allowing aerosol effects on cloud microphysics and radiation to feed back on the model meteorology, our estimates of the aerosol indirect effect do not include changes in relative humidity and cloud cover.

Citation: Storelvmo, T., J. E. Kristjánsson, S. J. Ghan, A. Kirkevåg, Ø. Seland, and T. Iversen (2006), Predicting cloud droplet number concentration in Community Atmosphere Model (CAM)-Oslo, *J. Geophys. Res.*, *111*, D24208, doi:10.1029/2005JD006300.

1. Introduction

[2] Over the past decades the radiative forcing due to anthropogenic aerosols has been recognized as crucial for our understanding of climate change caused by human activity. Anthropogenic aerosols have a direct effect on the radiative balance of the Earth through scattering and absorption of solar radiation. In addition, the aerosols have an indirect effect on the radiative balance through clouds as they can act as cloud condensation nuclei (CCN) and thereby alter the cloud albedo and precipitation processes [*Rosenfeld et al.*, 2002]. The two main processes by which aerosols modify clouds are known as the first indirect effect (alternatively, Twomey effect [*Twomey*, 1977]) and the second indirect effect (alternatively, Albrecht effect [*Albrecht*, 1989]), respectively. The first effect refers to an increase in cloud albedo as cloud droplets become smaller as a result of increased CCN and cloud droplets number concentrations (CDNC). The latter effect refers to the less efficient precipitation release as cloud droplets become smaller, leading to increased cloud liquid water content and possibly also lifetime. In addition, there are several hypotheses on other processes through which anthropogenic aerosols interact with clouds. The effect of an absorbing black carbon (BC) layer is one example, also known as the semidirect effect [*Hansen et al.*, 1997]. BC absorption of solar radiation can affect the vertical profiles of temperature and relative humidity and thereby potentially influence cloud formation and dissipation. As these other processes are still relatively unknown, this study will focus only on the first and second indirect effect.

[1] Department of Geosciences, University of Oslo, Oslo, Norway.
[2] Pacific Northwest National Laboratory, Richland, Washington, USA.

0148-0227/06/2005JD006300$09.00

[3] Sulfate and carbonaceous aerosol concentrations have increased since preindustrial time because of human activities such as biomass burning and fossil fuel combustion [*Charlson*, 1988; *Penner et al.*, 2001]. While sulfate particles are highly hygroscopic and frequently act as CCN, elemental carbon is practically hydrophobic, implying that the ability of BC to act as CCN is fairly poor. However, when internally mixed with, e.g., sea salt or sulfate, BC can still take part in cloud droplet activation. Organic aerosols are generally a complex mixture of hundreds or even thousands of different organic compounds with varying hygroscopic properties [*Kanakidou et al.*, 2005]. Hence their hygroscopic properties must currently be treated empirically in model studies. In this study organic carbon (OC) particles are assumed to be slightly hygroscopic, meaning that they can act as CCN at high supersaturations when externally mixed. Lately, studies have concluded that when coated with sulfate, particulate organic matter may be highly soluble in water [*Lohmann et al.*, 2004]. Hence organic aerosols potentially play an important role in cloud droplet activation when internally mixed, even with fairly small amounts of sulfate or sea-salt.

[4] Both the direct and indirect effects of aerosols are estimated to cool the current climate, although both effects are quantitatively highly uncertain. The third assessment report of the Intergovernmental Panel on Climate Change (IPCC) concluded that the two effects combined could, according to the highest estimates, practically cancel the warming caused by an increase in greenhouse gases. However, the global warming trends over the last two centuries indicate that the highest estimates may be unrealistic [*Penner et al.*, 2001]. The uncertainty associated with the effect of aerosols on clouds is the motivation for this study. The indirect effects of aerosols on ice clouds are not taken into consideration in this paper. However, a similar framework to the one for liquid clouds presented in this paper is under development for such clouds.

[5] The following section (section 2) will describe CAM-Oslo and each of the modules working together in the framework for calculations of the aerosol indirect effect. The framework consists of four modules: The aerosol life cycle module (module 1), the aerosol size distribution module (module 2), the cloud droplet activation module (module 3) and the microphysical cloud droplet sink module (module 4). The new continuity equation will also be described in the following section. The results produced by the framework will be presented in section 3, while section 4 contains three sensitivity experiments. The results are discussed in section 5 and section 6 contains a conclusion and plans for future studies of aerosol cloud interactions.

2. Framework

[6] The framework presented here for calculating the aerosol indirect effect (hereafter AIE) is an extension of the framework presented by *Kristjánsson* [2002]. Significant improvements of the framework have been carried out, the most important ones being the inclusion of OC, improved treatment of supersaturation and the implementation of a continuity equation for CDNC. To calculate both the radius and lifetime effects as radiative forcings, two parallel calls are made to the radiation and cloud microphysics schemes [*Slingo*, 1989; *Rasch and Kristjánsson*, 1998] of the model at every time step. One is for advancing the model, the other one is a diagnostic call. It corresponds to microphysical properties based on natural aerosols or all (natural + anthropogenic) aerosols, depending on emission scenario (preindustrial or present-day, respectively). For details, see *Kristjánsson* [2002]. In the following subsections, the host model and the modules implemented to form CAM-Oslo are presented, the new parameterizations being described in subsection 2.4 and 2.6.

2.1. NCAR CAM-2.0.1

[7] CAM-Oslo is a modified version of NCAR CAM-2.0.1 (http://www.ccsm.ucar.edu/models/). In this study the model was run with an Eulerian dynamical core, 26 vertical layers and a horizontal resolution of $2.8° \times 2.8°$. The dynamical time step is 20 min. The model runs with a land surface model and climatological sea surface temperature and sea ice conditions. Modules for calculations of the direct and indirect effect of aerosols have been added to the host model. In the following subsections, the modules concerning the AIE will be presented. The framework for calculation of the direct effect of aerosol is presented by *Kirkevåg and Iversen* [2002]. We have chosen to calculate pure radiative forcings rather than quasi-forcings to avoid the noise problem introduced once the calculated AIE is allowed to feed back on the model. The framework described in the following sections is applied only to stratiform clouds in the model. The stratiform cloud cover in CAM-Oslo depends on relative humidity and atmospheric stability. As we have chosen not to allow aerosol effects on cloud microphysics and radiation to feed back on the model meteorology, we will not be able to simulate any aerosol effects on cloud cover in this study.

2.2. Module 1: Aerosol Lifecycle Module

[8] A process-oriented lifecycle model for sulfate and carbonaceous aerosols has been developed by *Iversen and Seland* [2002]. The lifecycle scheme includes emissions of dimethyl sulfide (DMS), SO_2 and sulfate, and also emissions of BC and OC from biomass burning and fossil fuel combustion. Gas phase and aqueous phase aerosol chemistry, coagulation and dry and wet deposition are also treated by the scheme, accounting for the entire lifecycle of these aerosol species in the atmosphere. By running this lifecycle model interactively in our AIE simulations, vertical and horizontal distributions of sulfate and carbonaceous aerosols are obtained in response to the changing meteorological conditions. We believe the interactivity, although computationally expensive, to be an important step toward more realistic aerosol distributions. Compared to *Kristjánsson* [2002], the temporal resolution is significantly improved, as monthly mean aerosol concentrations were used in that study. Sea salt and mineral dust aerosols are not included in the model as prognostic variables, meaning that they are not subject to transport, coagulation and deposition. These aerosols are treated as background aerosols, their size distributions being prescribed according to surface properties and latitude. The sulfate and carbonaceous aerosols can be both internally and externally mixed

with the background aerosol, as will be described in the following section.

2.3. Module 2: Aerosol Size Distribution Module

[9] In the aerosol size distribution module, the sulfate, BC and OC aerosol concentrations obtained from the aerosol life cycle module are combined with the background aerosol following the methodology developed by *Kirkevåg and Iversen* [2002]. The background size distributions applied in this methodology are based on the work presented by *Kirkevåg et al.* [2005] and are described in detail there. The module treats five different background aerosol types, each consisting of multiple aerosol components. Each component can be associated with a mode in a multimodal lognormal size distribution. The five background aerosol types are (1) *Continental*, consisting of one mode of internally mixed mineral dust and sea salt and two pure mineral modes (fine and coarse), (2) *Maritime*, consisting of one mineral mode and three sea salt modes (fine, accumulation, and coarse mode, respectively), (3) *Desert*, consisting of fine and coarse mineral modes, (4) *Arctic*, consisting of a fine mineral mode and a sea salt accumulation mode, and (5) *Antarctic*, consisting of a mineral mode and a two sea salt modes (fine and accumulation).

[10] Both the aerosol size distribution and composition are modified as sulfate, OC, and BC are internally mixed with the background aerosol. The modes in the size distributions will typically not be lognormal after the modification. The size distribution is described by a set of 44 bins on a logarithmic r-axis, with radii (r) ranging from 0.001 to 20 μm. OC, BC and sulfate are also allowed to be externally mixed with the background in lognormal nucleation modes. The background aerosol is ''quasi-transported'', meaning that the fine mineral modes and sea salt modes are transported in accordance with the predominant zonal wind direction.

2.4. Module 3: Cloud Droplet Activation Module

[11] Within the cloud droplet activation module the aerosol fraction activated to form cloud droplets is determined. This module is based on an algorithm developed by *Abdul-Razzak and Ghan* [2000]. The activation algorithm can treat monomodal and multimodal lognormal size distributions as well as sectional size distributions [*Abdul-Razzak et al.*, 1998; *Abdul-Razzak and Ghan*, 2002]. The sectional approach would be the ideal application for the size distributions calculated in module 2. However, in order to save computational time we were forced to choose the algorithm treating multimodal size distribution. Although the background aerosol size distributions consist of multiple lognormal modes, the modes are no longer lognormal after the addition of sulfate, BC and OC. We chose to solve this by calculating the best lognormal fit to each of the modes in every grid box and for every time step. Offline comparisons between original size distributions and recalculated size distributions have been carried out, and results from these comparisons will be presented in section 3.2. The activation scheme calculates the activated aerosol fraction for each of the modes in the size distribution. This fraction is calculated on the basis of the hygroscopic properties of each mode (which can consist of one or more components), and a subgrid distribution of vertical velocity. The latter is obtained using the parameterization presented by *Ghan et al.* [1997]. The distribution is centered around the grid box vertical velocity, $\overline{w}$, while the standard deviation, σ_w, is calculated using the following formula:

$$\sigma_w = \frac{\sqrt{2\pi}K}{\Delta z} \quad (1)$$

where K is the vertical eddy diffusivity and Δz is the model layer thickness. For a coarse vertical resolution, as in GCMs, σ_w is typically underestimated. A lower bound for σ_w is therefore necessary, in this study it is set to 30 cm/s. The activation scheme also takes into account the so-called competition effect [*Ghan et al.*, 1998]. Each CCN must compete with all other CCN for the water vapor needed for activation into stable cloud droplets. This competition limits the maximum supersaturation in an updraft. Hence the activation of a given CCN is highly dependent on the presence of other CCN particles. The influence of the competition effect on the AIE is investigated in section 4.1.

[12] The parameterization of the nucleation term largely follows *Ghan et al.* [1997]. The nucleation term is calculated differently depending on the age of the cloud. Clouds that last longer than one numerical time step, i.e., longer than 20 min, are considered old or long-lived clouds. If a cloudy grid box was cloud-free the previous time step the cloud is considered new.

[13] For new clouds, the CCN fraction activated is determined from the updraft velocity spectrum and aerosol properties using the activation algorithm. For old clouds, we also apply the activation algorithm but assume that new droplets form only when the number activated from the algorithm exceeds the preexisting CDNC, following *Lohmann et al.* [1999]. Hygroscopic properties for each aerosol type are taken from *Ghan et al.* [2001], with the exception that we assume a lower fraction of mineral dust to be soluble (0.013). The sensitivity of our results to varying the soluble fraction of mineral dust is tested in a sensitivity study presented in section 4.3.

2.5. Module 4: Microphysical Source/Sink Module

[14] The number concentration of cloud droplets activated per unit time within Module 3 corresponds to the source/nucleation term in the continuity equation for CDNC. The continuity equation also consists of several microphysical sink terms for CDNC. Cloud droplets can be lost through evaporation, precipitation processes or through self-collection. Self-collection is the process in which cloud droplets collide and stick together, but do not reach the size where they precipitate out. The self-collection term is calculated on the basis of the parameterization developed by *Beheng* [1994]. A new feature in NCAR CAM-2.0.1 compared to previous NCAR model versions is a cloud microphysics scheme developed by *Rasch and Kristjánsson* [1998]. The scheme includes a prognostic equation for cloud liquid water mixing ratio:

$$\frac{dq_l}{dt} = Aq_l + Cond. - PWAUT - PRACW - PSACW - E \quad (2)$$

q_l: cloud liquid water mixing ratio;
A_{ql}: transport (convection and turbulence);
Cond.: condensation of cloud liquid water;
PWAUT: autoconversion of cloud droplets;
PRACW: collection of cloud droplets by rain drops;
PSACW: collection of cloud droplets by snow;
E: evaporation of cloud water (liquid phase).

[15] In this study, we have assumed a direct proportionality between the loss of cloud water and loss of cloud droplets for precipitation processes. We assume two possible scenarios for evaporation; We evaporate cloud droplets if the cloud is shrinking. The cloud droplet percentage lost then equals the percentage of the cloud that is lost. Cloud droplets are also lost through evaporation when the relative humidity sinks below a threshold value. Cloud water is then evaporated until the threshold value is reached or until the entire cloud has evaporated. Cloud droplets are in this case lost in proportion to the cloud water evaporated. The precipitation term is divided into an autoconversion term and two collection terms; one where liquid cloud droplets are collected by rain drops and another where they are collected by precipitating snow. The autoconversion (*PWAUT*) is given by

$$PWAUT = \left[\left(C_{l,aut} q_l^2 \rho_a\right)/\rho_w\right] \cdot \left[(q_l \rho_a)/(\rho_w N_l)\right]^{1/3} \cdot H(r_{3l} - r_{3lc}) \quad (3)$$

ρ_a: air density;
ρ_w: water density;
r_{3l}: mean volume radius;
r_{3lc}: critical mean volume radius;
H: heaviside function (1 if $r_{3l} \geq r_{3lc}$, 0 otherwise).

[16] Here the proportionality factor $C_{l,aut}$ and the critical value for cloud droplet mean volume radius are both relatively uncertain parameters [*Kristjánsson*, 2002]. In this study we chose to adopt a critical value for cloud droplet mean volume radius (r_{3lc}) of 15 μm, while $C_{l,aut}$ is a constant dependent on the precipitation rate. As previous studies have found the AIE to be sensitive to variations in r_{3lc}, we have carried out a sensitivity study investigating this in our model (section 4.2).

2.6. Continuity Equation for CDNC

[17] The four modules described above give us the terms on the right hand side of the new continuity equation:

$$\frac{dN_l}{dt} = A_{N_l} + Nucl - \frac{N_l}{q_l}(PWAUT + PRACW + PSACW + E_1) - E_2 - Self - Freez \quad (4)$$

N_l: cloud droplet number (Number/cm^3);
A_{Nl}: transport (convection and turbulence);
q_l: mixing ratio for cloud water (liquid phase);
Self: rate of self-collection of cloud droplets (i.e., coalescence of cloud droplets not resulting in precipitation);
Freez: freezing of cloud droplets to form ice crystals;
E_1: evaporation of cloud droplets for RH < 100%;
E_2: evaporation of cloud droplets for shrinking cloud.

[18] Equations for cloud droplet conservation similar to equation (3) have previously been introduced by *Ghan et al.* [1997] and *Lohmann et al.* [1999]. The importance of the different terms (nucleation, evaporation, precipitation and self-collection) as a function of latitude and height will be discussed in section 3.3. Cloud droplets are formed and depleted in proportion to the liquid fraction of the cloud in each grid box. The freezing term in equation (4) simply makes sure that if the temperature drops below −20°C in a cloudy grid box, all cloud droplets are frozen. In this study, cloud droplets are not advected in the model, so consequently A_{Nl} here represents only vertical transport of cloud droplets through convection and vertical diffusion. This approach is consistent with cloud water not being an advected constituent in NCAR CAM2.0.1. As the typical lifetime of a cloud in NCAR CAM2.0.1 is only a couple of time steps, we do not believe horizontal transport to be important. However, when implementing this framework in the newest NCAR model version both cloud water and droplets will be advected, and we will get and indication of the importance of this term.

3. Model Results

[19] In this section, our model results will be presented and discussed in the context of observations and estimates from other model studies. Additionally, we attempt to quantify the effects of critical model assumptions.

3.1. Anthropogenic Changes in Aerosol Column Burdens

[20] The aerosol indirect effect comes about because of anthropogenic changes in aerosol burdens since preindustrial times. Consequently, we must consider our modeled aerosol indirect effect in light of the modeled anthropogenic changes of the different aerosol species.

[21] The anthropogenic change in sulfate column burden is highest over the Northern Hemisphere continents, as can be seen from Figure 1a. Three distinct maxima can be identified; over Southeast Asia, eastern United States, and over eastern Europe. As sulfate aerosols are efficient CCN, these areas are also expected to be associated with significant changes in CDNC, cloud droplet effective radii and SWCF. This is indeed the case, as will be discussed further in section 3.4. Sulfate, OC and BC column burdens from CAM-Oslo have been carefully validated against satellite observations and compared to other models within the Global Aerosol Model Intercomparison (AEROCOM) project (http://nansen.ipsl.jussieu.fr/AEROCOM/). The global averages for sulfate, BC and OC column burdens (from anthropogenic sources only) are 1.87, 0.12 and 0.74 mg/m^2, respectively. *Schultz et al.* [2006] compare aerosol burdens from 9 different GCMs and chemical transport models (CTMs) for AEROCOM B aerosol emissions. They find the average burdens to be 2.15, 0.25 and 1.38 mg/m^2 for sulfate, BC and OC, while the standard deviations were 0.83, 0.08 and 0.42, respectively. Hence our modeled anthropogenic sulfate burden compares well with these results, while our BC and OC numbers are low. As sulfate aerosols are believed to be the

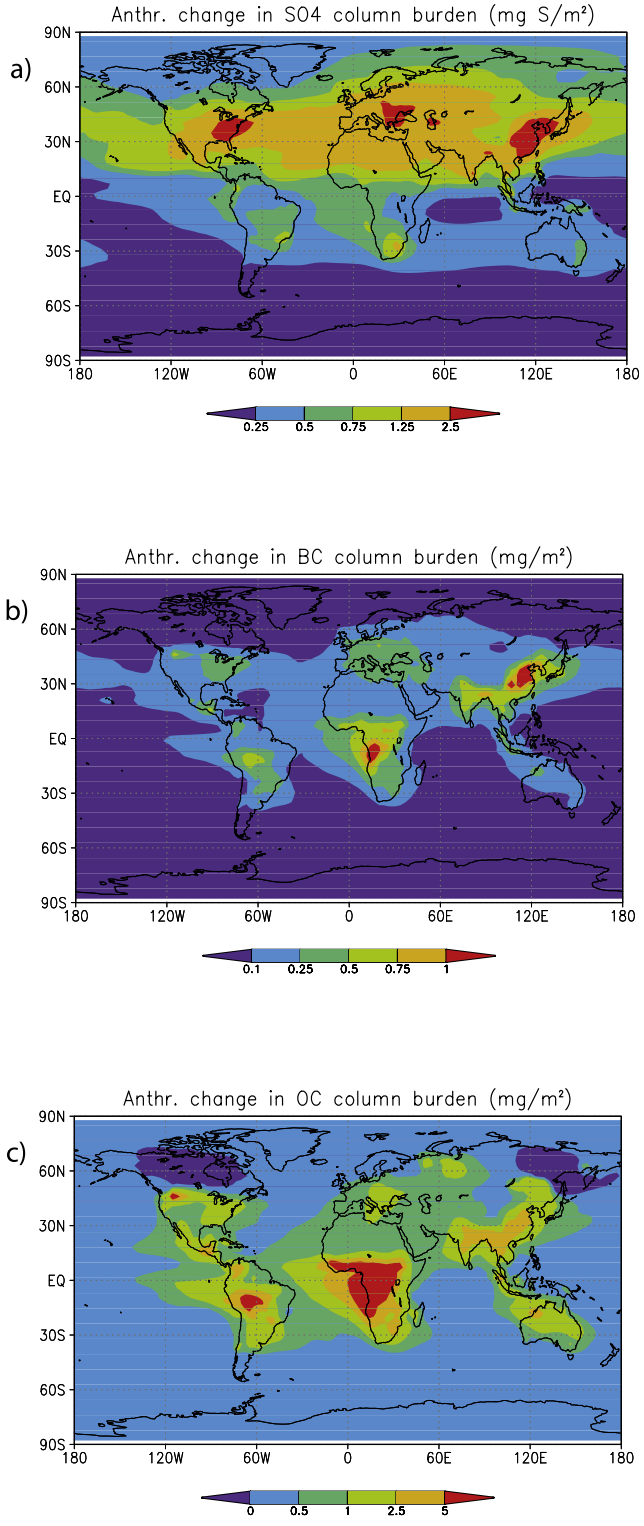

Figure 1. Change in column burdens due to anthropogenic aerosol emissions: (a) SO_4 (mg S/m^2). (b) BC (mg/m^2). (c) OC (mg/m^2).

most important anthropogenic aerosols in terms of the aerosol indirect effect, we don't expect this to affect our results significantly. However, we may underestimate the aerosol indirect effect particularly in biomass burning areas. The anthropogenic contribution to BC column burden (Figure 1b) has one pronounced maximum, over eastern China, associated with fossil fuel burning. A secondary maximum over equatorial Africa is most likely connected to biomass burning. BC aerosols are not taking part in cloud droplet nucleation unless internally mixed with more hygroscopic aerosol species. In the real atmosphere, high concentrations of BC would certainly affect the temperature profile and hence clouds through absorption of shortwave radiation. However, neither direct nor indirect effects of aerosols are allowed to affect the model meteorology in our simulations. Hence we do not expect significant changes in cloud parameters due to changes in BC column burden.

[22] The anthropogenic contribution to OC column burden (Figure 1c) is highest in equatorial western Africa, associated with areas of frequent biomass burning. Also in other areas with frequent biomass burning like South America and to some extent Asia, high values are found. Note the negative values at NH high latitudes. These areas are assumed to have been dominated by frequent forest fires in preindustrial times. OC is in this study assumed to be somewhat hygroscopic and hence should increase CDNC in areas with high anthropogenic column burden.

3.2. Lognormal-Fitting Approximation

[23] In this section, the effect of approximating each mode in the size distribution from module 2 with the best lognormal fit is evaluated. We have calculated the number of CCN activated into cloud droplets for a broad variety of conditions in both the original size distributions and the recalculated size distributions. Five parameters have been varied to form more than 5000 different combinations, and the results are given in Figure 2 as scatterplots for each background type. The varying parameters are (1) critical radius for cloud droplet activation (r_{cr}), (2) total mass of sulfate, OC and BC mixed internally with the background aerosols (C_{tot}), (3) carbonaceous fraction of C_{tot} (fc), (4) organic mass fraction of carbonaceous aerosols (foc), and (5) the internally mixed sulfate fraction originating from in-cloud oxidation (faq).

[24] A linear regression has been calculated for each background type on the basis of all parameter combinations. Ideally, the activated CCN for the recalculated size distributions (scatterplot x-axis) should equal the CCN activated in the exact size distributions (scatterplot y-axis), giving the straight line y = x. The deviation from ideality is quantified in Table 1, showing the results from a linear regression analysis for each background type. The best fitted straight line estimated from the least squares method is given by y = ax + b. The sample correlation coefficient is also given in Table 1. Relatively large deviations are found for the maritime and antarctic backgrounds, in particular when relatively many CCN are activated. Deviating data points often correspond to small critical radii for activation and high concentrations of internally mixed OC, BC and sulfate. As warm clouds hardly ever occur over Antarctica, this background is rather irrelevant for this study. The maritime background is however central as oceans cover approximately 70% of the Earth's surface. Strong in-cloud oxidation to form sulfate causes the initially lognormal background modes to become practically bimodal. Redis-

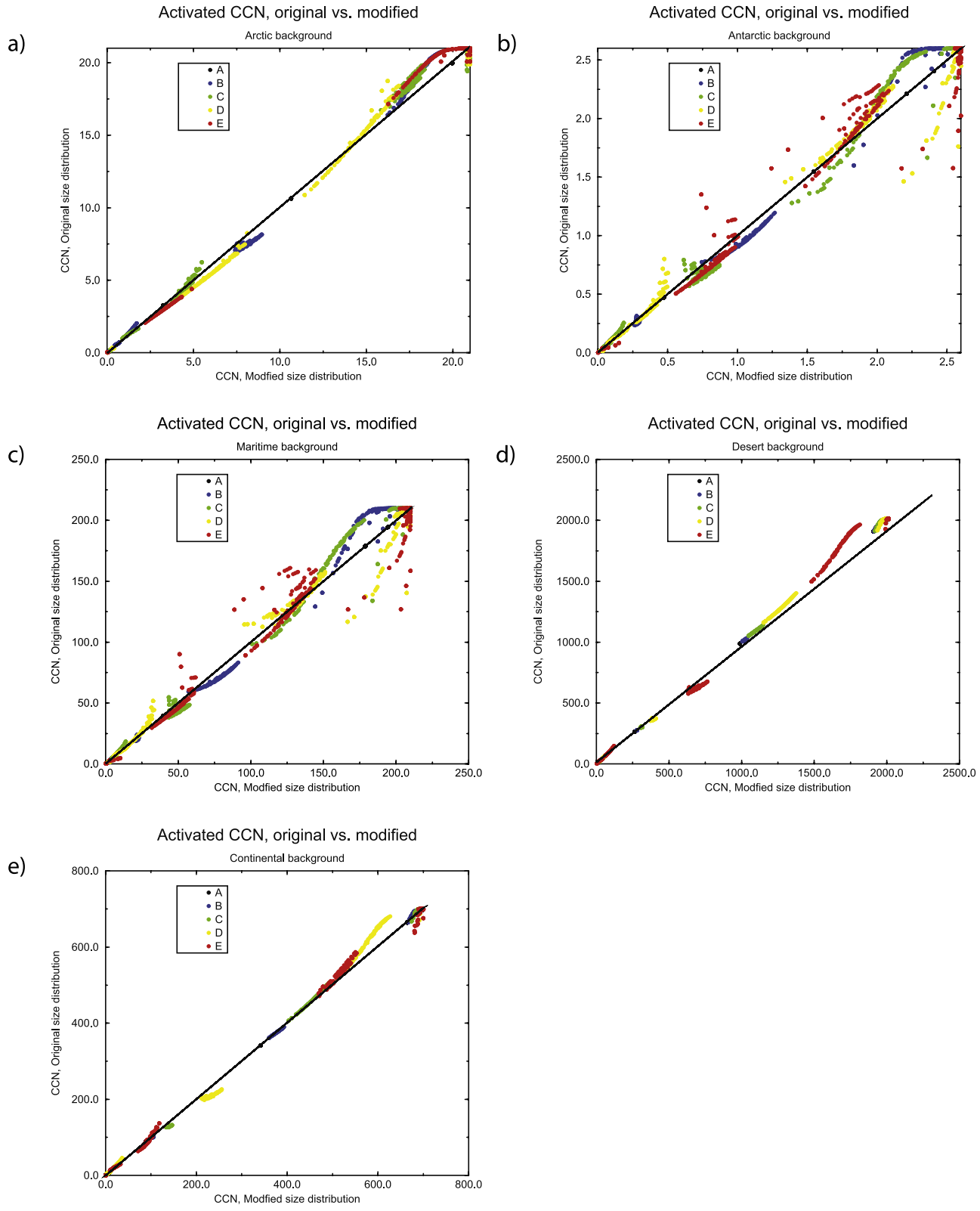

Figure 2. Scatterplots of CCN activated into cloud droplets for each background type for a number of values of C_{tot} (ranging from $1 \cdot 10^{-10}$ to 20 $\mu g/m^3$,), fc, foc, faq (all ranging from 0 to 1), and r_{cr} (ranging from 0.1 μm to 10 μm). Different colors correspond to different C_{tot} values, A representing the lowest value of C_{tot} and E representing the highest value. Abscissa: CCN activated in simplified size distribution. Ordinate: CCN activated in original size distribution. Each dot represents a parameter combination, lines are linear regressions to the data points.

Table 1. Results From Linear Regression Analysis of CCN Activated for Original and Simplified Size Distributions

Aerosol Type	Regression Constant a	Regression Constant b	Correlation Coefficient ρ
Continental	1.0044	−0.42	0.9997
Maritime	0.9994	−0.21	0.9965
Desert	0.9492	13.6	0.9913
Arctic	1.0069	−0.027	0.9992
Antarctic	0.9982	0.00	0.9963

tribution of the anthropogenic sulfate to form a single lognormal mode will lead to errors when faq is close to unity. However, the scatterplot does not reveal any systematic errors.

[25] In desert areas, the recalculated size distribution will slightly underestimate the CCN fraction activated. However, the deviation is small relative to the total aerosol number typically found in desert areas. In summary, we can assume that the lognormal approximation is not introducing any systematic errors in the GCM simulations and that it is therefore an acceptable simplification.

3.3. Importance of Each Term in the Continuity Equation for CDNC

[26] Figure 3 shows the importance of each term in the continuity equation as a function of height and latitude. The terms are averaged over one year from a model run with present day aerosol emissions. Both sources and sinks are given per time step, i.e., the cloud droplet number lost or gained over a period of 20 min. As apparent in Figure 3a, cloud droplet nucleation is significantly higher in the Northern Hemisphere (NH) than in the Southern Hemisphere (SH) at all levels. This is to be expected as continents

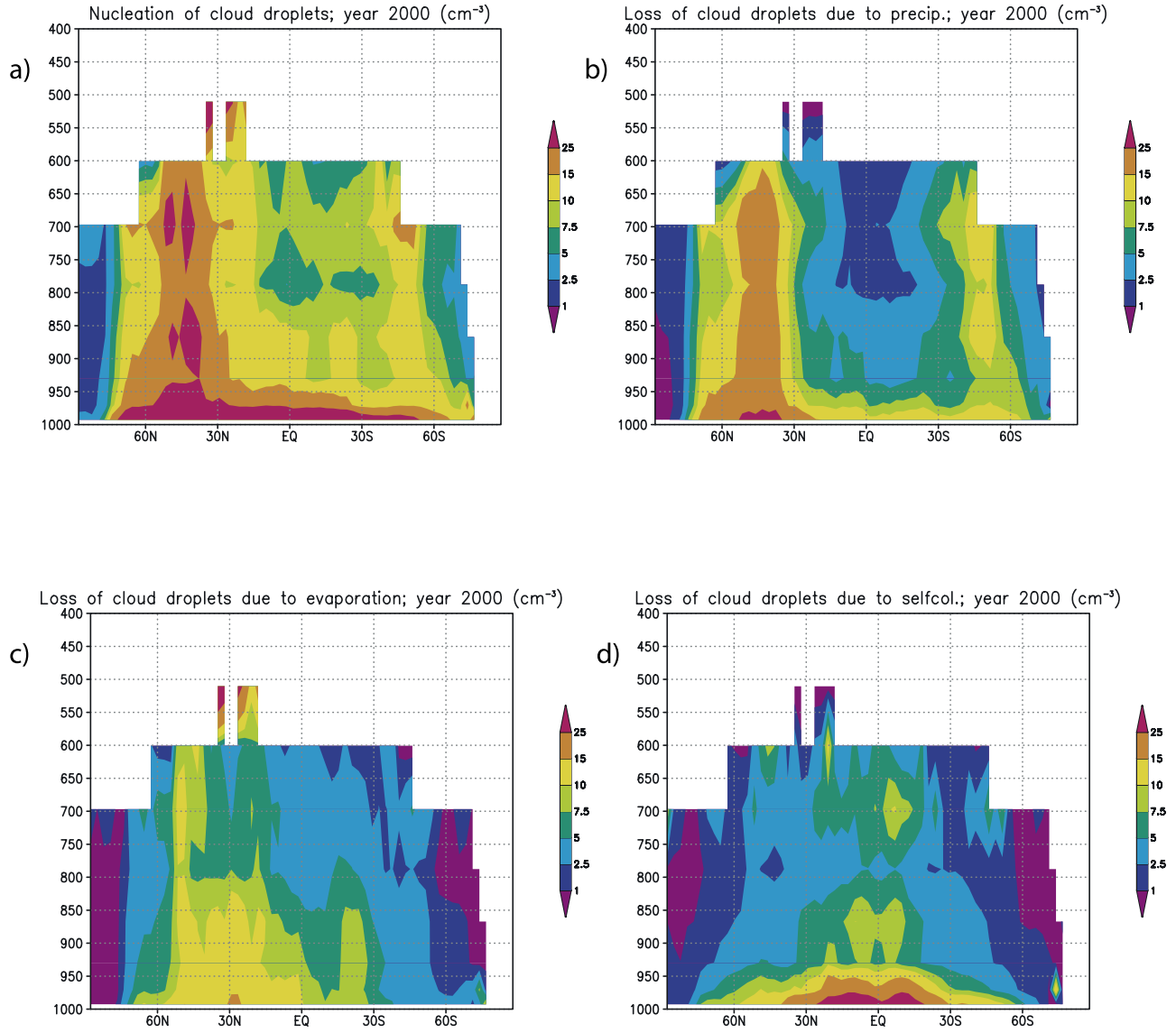

Figure 3. Zonally averaged cross section of sources and sinks for CDNC per time step (20 min). (a) Nucleation of cloud droplets. (b) Loss of cloud droplets due to precipitation processes (i.e., autoconversion and accretion by raindrops and snow crystals). (c) Loss of cloud droplets due to evaporation. (d) Loss of cloud droplets due to self-collection.

cover more surface in NH and aerosol emissions are higher. For all latitudes we find maxima in cloud droplet nucleation just above ground, where the aerosol number concentration is high. Hence as the clouds form, a high number of CCN are activated. A secondary maximum can be seen at approximately 700 hPa. This corresponds to the maximum in grid box in-cloud vertical velocity which is central in our cloud droplet activation parameterization. Convective transport of aerosols capped at approximately 550 hPa can be the explanation for the maximum in nucleation rate seen at this height. As pointed out by *Menon et al.* [2002], the cloud frequency of occurrence in the lowermost model layers can potentially have a strong influence on the simulated AIE. A high frequency of low-cloud occurrence would be expected to lead to a stronger AIE as aerosol concentrations (of both natural and anthropogenic origin) are typically highest close to the surface and decrease rapidly with height. The three lowest model levels in CAM-Oslo have cloud tops at approximately 985hPa, 956hPa and 903hPa. Warm cloud frequencies of occurrence for these levels are 24.8%, 30.6% and 36.4%, respectively. These numbers are comparable to those reported for the lowest model layers by *Menon et al.* [2002]. Unfortunately, satellite estimates of this quantity are highly uncertain.

[27] Figure 3b shows the loss of cloud droplets due to precipitation processes, i.e., due to autoconversion and cloud droplet collection processes. Precipitation processes are important sinks for cloud droplets, especially up to 600 hPa in midlatitude storm tracks.

[28] Evaporation is the dominating sink for cloud droplets at high altitudes (Figure 3c). At low altitudes, the maximum evaporation occurs at around 30°N. As evaporation is either proportional to the loss in cloud water or cloud fraction, it is to be expected that a cloud with high CDNC will also correspond to high evaporation loss of cloud droplets.

[29] Self-collection depletes cloud droplets efficiently near the ground (Figure 3d). This is to be expected as self-collection is parameterized as a function of the cloud liquid water content, which is highest at low levels and decreases rapidly with height. At higher levels self-collection is practically negligible, except in the tropics where convection transports cloud water aloft.

3.4. Simulated Aerosol Indirect Effect (AIE)

[30] In this section the results of a 3-year control run are presented and compared to satellite observations. The control run is carried out with aerosol emissions corresponding to present day (PD) conditions. Also presented are differences between the control run and a model run carried out for emissions corresponding to preindustrial (PI) conditions. As we let the model state evolve independently of the aerosols, only a short spin up of a few months is assumed for the model runs. We define the AIE as the difference in CRF at the top of the atmosphere (TOA) between the control run and the PI run. The net CRF is the sum of the shortwave and longwave component of the radiative forcing (SWCF and LWCF, respectively). The difference in CRF is due to differences in cloud droplet effective radius (r_e) and cloud liquid water path (LWP). Changes in r_e affect only the SWCF budget, while the change in LWP affects both shortwave and longwave cloud forcing. Both parameters are changed because of a difference in CDNC between the two model runs. Figure 4a shows the column CDNC for the control run, while Figure 4b shows the corresponding International Satellite Cloud Climatology Project (ISCCP) observations from *Han et al.* [1998]. Both the model and the satellite observations show a strong land to sea contrast. Modeled values are slightly higher than the satellite observations over the subtropical ocean, while the opposite is true for midlatitude oceanic areas. Biomass burning aerosol contribution to CDNC seems to be somewhat underestimated in the model as observed column CDNC maxima are less pronounced in the model. As expected, areas yielding high CDNC correspond to continental areas with heavy aerosol loading, with maxima of more than $20 \cdot 10^6 \mathrm{cm}^{-2}$. As the mean vertical velocity in a model grid box is typically close to zero, the standard deviation of the subgrid distribution of w is by large determining the maximum supersaturation reached. Therefore areas with high σ_w should also yield high CDNC, e.g., the North American West Coast and the Andes. Although dust particles are assumed to be only slightly soluble in our control run (soluble fraction of 1.3%), the column CDNC values over the African deserts are still fairly high. This can be explained by the internal mixing with more soluble aerosol species. As evident from Figure 1a, pollution from Europe is transported across the Mediterranean Sea toward northern Africa and can contribute to high CDNCs there. As the aerosol number concentration is very high in these areas, the fraction activated does not have to be very high in order to get high CDNCs. However, column CDNC values over the African deserts are even higher in the satellite observations. These high values are possibly due to dust contamination, as discussed by *Menon et al.* [2002]. Areas corresponding to low-column CDNC are the subtropical oceanic areas, the Pacific in particular. Arctic and Antarctic areas are very clean and have low-column CDNC values, as expected. In the Arctic values are below $2 \cdot 10^6 \mathrm{cm}^{-3}$ everywhere, while the Antarctic continent does not experience warm clouds at all in this model run.

[31] Figure 4c shows the change in column CDNC due to anthropogenic aerosols, i.e., the difference between the control run and the PI run. Areas of high values correspond very well with areas of high-anthropogenic sulfate and OC loading shown in section 3.1. Transport of Saharan dust across the Atlantic seems to be well represented by the quasi-transport algorithm, resulting in an anthropogenic plume of high column CDNC off the African western coast when the dust is internally mixed with biomass burning aerosols.

[32] Figures 5a and 5b show the modeled cloud droplet effective radius sampled similarly to satellite retrievals and the corresponding ISCCP observations from *Han et al.* [1994]. In the model, finding the effective radius as seen from satellite simply implies searching from above in each model column for the highest liquid cloud (if any) which is optically thick with respect to longwave radiation, and record the effective radius of this cloud. This is done in order to be able to compare the modeled cloud droplet effective radii to the satellite observations. Minimum values are by large located in regions corresponding to high CDNC concentrations. These areas have cloud droplet effective radii down to less than 8 μm. However, as the cloud droplet effective radius is as dependent on the cloud liquid water

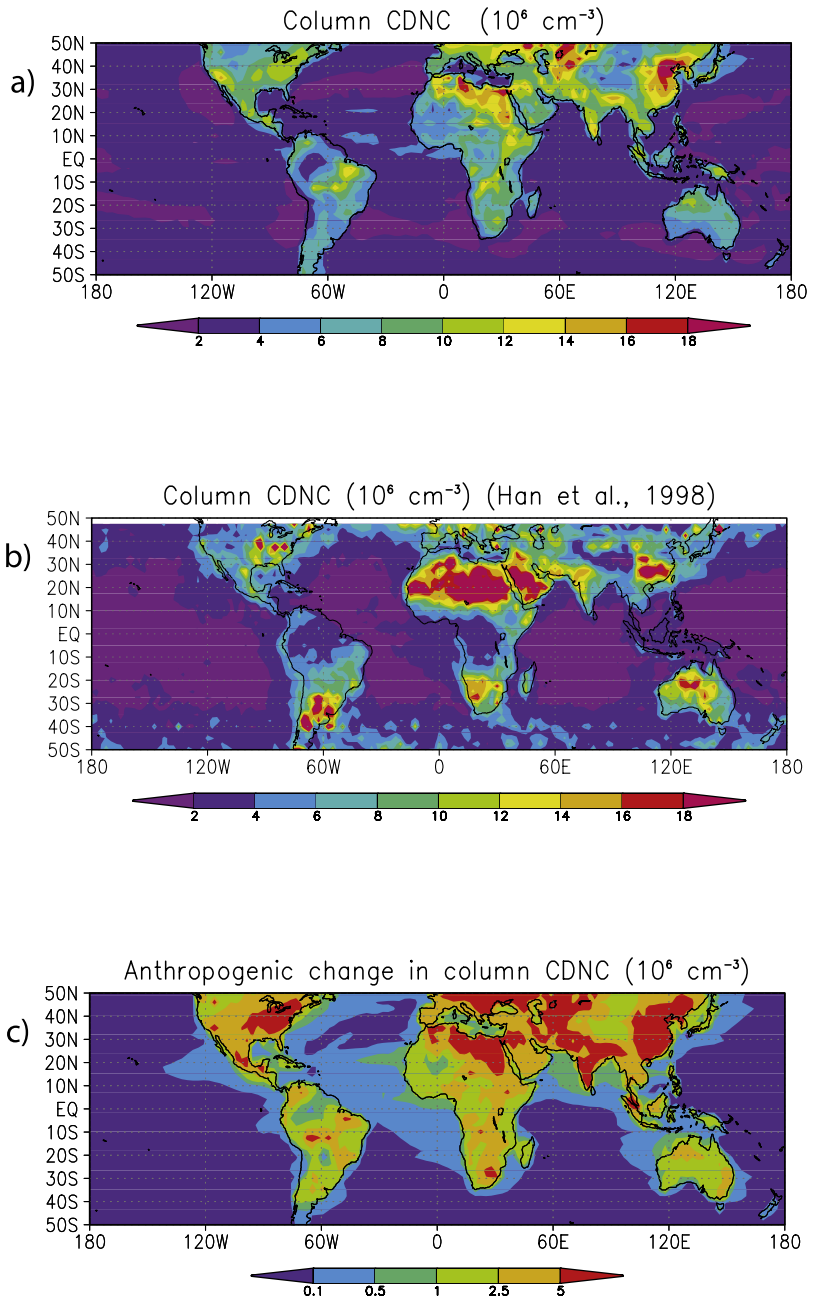

Figure 4. (a) Simulated column cloud droplet number concentration (CDNC) (10^6 cm^{-2}). (b) Column CDNC observed by satellite [*Han et al.*, 1998]. (c) Change in column CDNC due to anthropogenic aerosol emissions.

content (LWC) as on CDNC, small droplets should also be found in particularly dry areas. Desert areas and to some extent the interior of continents will therefore correspond to small cloud droplets. Subtropical oceans and arctic areas yield large cloud droplets with effective radii typically around 14–16 μm. The land to sea contrast seems to be somewhat underestimated and the effective radii are overall larger in CAM-Oslo than in the observations. However, compared to observations of the same parameter from the Moderate Resolution Imaging Spectroradiometer (MODIS) [*Storelvmo et al.*, 2006], CAM-Oslo values are too small.

[33] It should be pointed out that the shortwave radiation algorithm in NCAR CAM2.0.1 can only handle cloud droplet effective radii between 4 and 20 μm [*Slingo*, 1989]. Hence effective radii outside this interval are adjusted up/down to acceptable values. As cloud droplets outside this size interval are observed in the atmosphere, this is not ideal. Figure 5c shows the change in the effective radius as seen from satellite between the control run and the PI run. Again, maximum changes correspond very well with areas of high sulfate and OC aerosol loadings.

[34] Figures 6a and 6b show the cloud liquid water path (LWP) from the model and from the special sensor microwave imager (SSM/I) instrument [*Weng and Grody*, 1994]. Satellite data from the SSM/I instrument are only available over the oceans. Spatial patterns are overall quite similar in

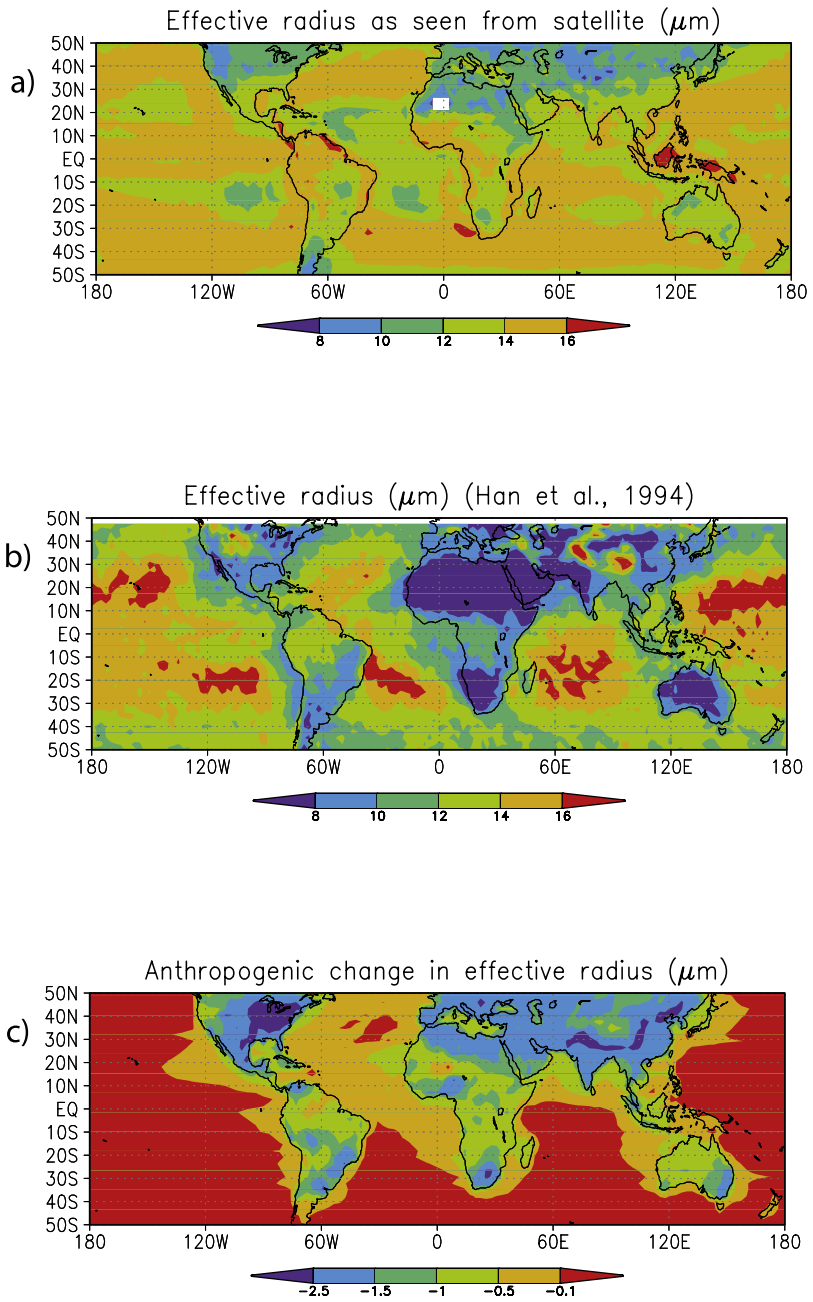

Figure 5. (a) Simulated cloud droplet effective radius (r_{eff}) as observed by satellite (μm). (b) r_{eff} from satellite observations [*Han et al.*, 1994] (c) Change in r_{eff} due to anthropogenic aerosol emissions.

the model and the observations, but CAM-Oslo values are slightly higher everywhere. As another analysis of the same satellite data set resulted in significantly higher values [*Greenwald et al.*, 1993], a qualitative comparison is more interesting than a quantitative one. Figure 6c shows the change in LWP due to anthropogenic aerosols. Areas of large anthropogenic changes in CDNC do not necessarily correspond to areas of large anthropogenic LWP changes. An example is northern Africa, where column CDNC changes quite significantly between the control run and the PI run. However, the area is extremely dry and cloud droplet radii are typically significantly smaller than the critical radius for the onset of autoconversion for both PI and PD conditions. Areas of maximum anthropogenic changes in LWP are typically areas with both relatively high precipitation rates (e.g., the midlatitude storm tracks) and high anthropogenic changes in CDNC. Figures 7a and 7b show the shortwave cloud radiative forcing (SWCF) from the model and from the Earth Radiation Budget Experiment (ERBE), respectively. The simulated SWCF is in fair agreement with the satellite observations, except for a slight underestimation in the subtropics. A similar bias was found and discussed by *Rasch and Kristjánsson* [1998] for a previous NCAR model version, NCAR CCM3. The anthropogenic change in SWCF is given in Figure 7c. As the anthropogenic change in LWCF is small in our simulations (global average of less than 0.01 W/m^2), the change in SWCF at the top of the atmosphere (TOA) practically equals the AIE. As this change comes about

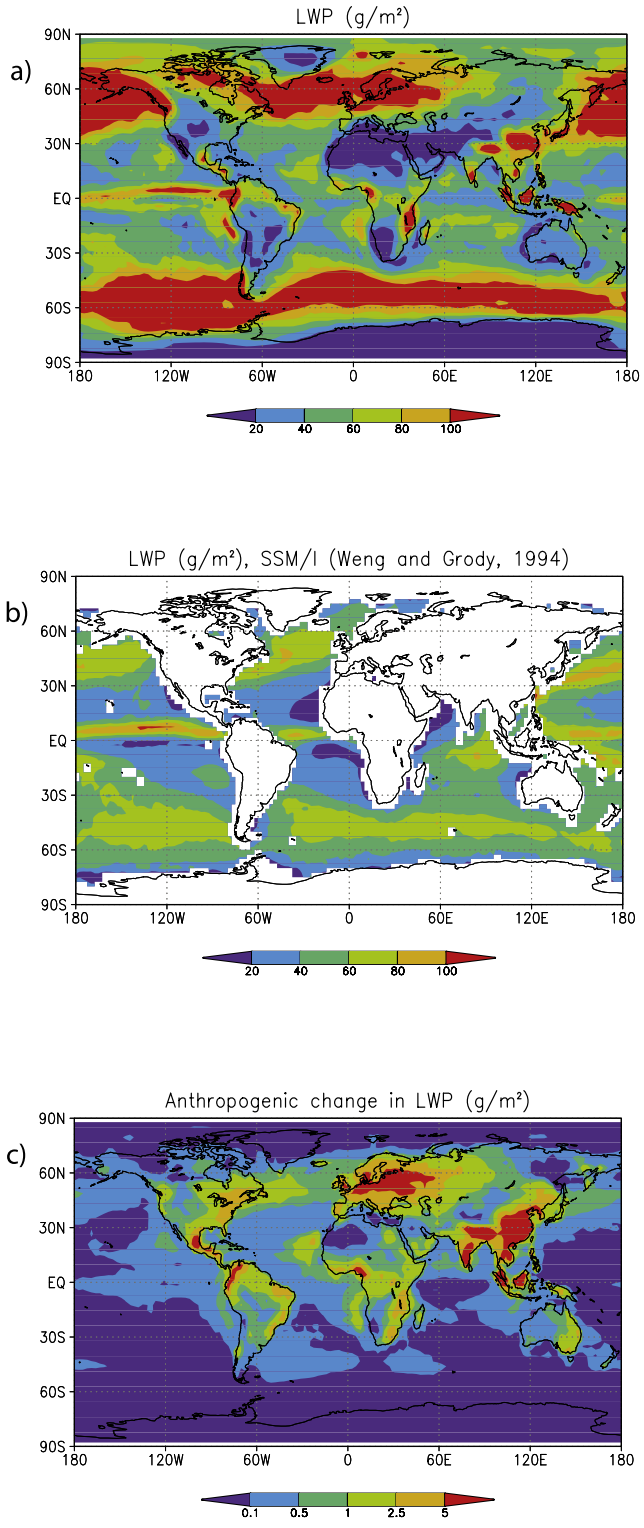

Figure 6. (a) Simulated cloud liquid water path (LWP) (g/m^2). (b) LWP observed by satellite [*Weng and Grody*, 1994]. (c) Change in LWP due to anthropogenic aerosol emissions.

because of changes in effective radius and LWP, high values should correspond to maxima in Figures 5c and 6c, which is also the case. The global average change in SWCF is -0.3W/m^2, hence the control run gives an AIE of -0.3W/m^2.

The parameters shown in Figures 4–7 are summarized in Table 2 in terms of global, NH, SH, oceanic and continental means.

[35] As expected, NH corresponds to larger anthropogenic changes in SWCF, r_{eff}, and LWP than SH because of the

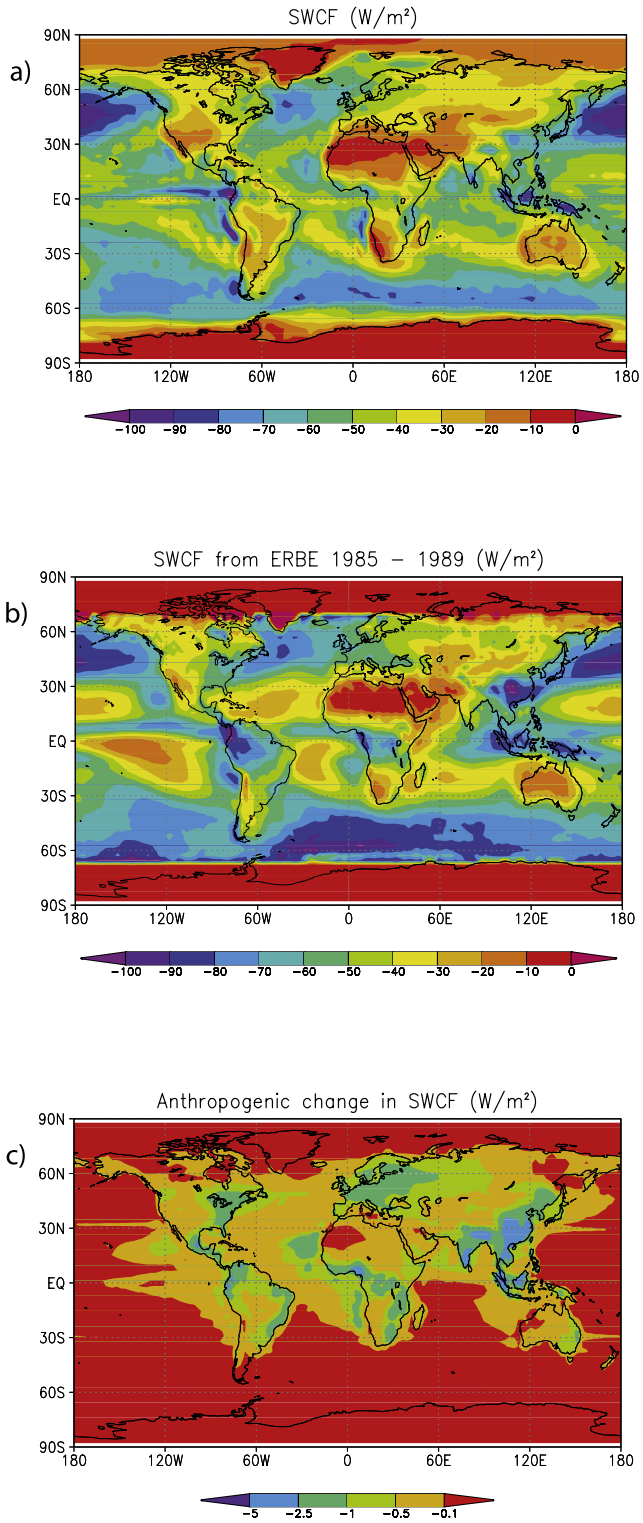

Figure 7. (a) Simulated shortwave cloud radiative forcing (SWCF) for aerosol emissions corresponding to present day (W/m^2). (b) SWCF observed by satellite (ERBE). (c) Change in SWCF due to anthropogenic aerosol emissions.

Table 2. Area and Annual Averages of Key Quantities

	Indirect Effect, W/m^2	r_{eff}, μm	LWP, g/m^2	Δr_{eff}, μm	ΔLWP, g/m^2
All, global	−0.30	13.3	61.5	−0.40	0.68
All, NH	−0.47	13.0	61.3	−0.59	1.06
All, SH	−0.13	13.7	61.8	−0.18	0.28
Ocean, global	−0.13	14.3	66.2	−0.15	0.25
Ocean, NH	−0.26	14.0	64.5	−0.24	0.42
Ocean, SH	−0.04	14.3	67.5	−0.08	0.14
Land, global	−0.68	11.5	50.7	−0.96	1.64
Land, NH	−0.77	11.6	56.7	−1.11	2.00
Land, SH	−0.46	10.9	38.1	−0.58	0.91

location of the aerosol source regions. Similarly, anthropogenic changes are larger over land than over the ocean. Consequently, the largest AIE, Δr_{eff} and ΔLWP are found in NH continental areas, and the smallest values are found in SH oceanic areas. r_{eff} ranges from 10.9 μm over land in NH to 14.3 μm over SH ocean, while the LWP is higher over ocean than over land.

4. Sensitivity Experiments

4.1. Difference Between Prescribed and Diagnosed Supersaturation

[36] In this sensitivity experiment we prescribed the supersaturation instead of calculating it, following the approach of *Kristjánsson* [2002]. A supersaturation of 0.05% was assumed for stratiform clouds, while convective clouds were given a supersaturation of 0.25% over ocean and 0.5% over land. By forcing the supersaturation to be the same in a polluted and a clean cloud, the influence of the competition effect on the AIE is investigated in a simplified manner.

[37] An aerosol indirect effect of −0.48 W/m^2 was found in this experiment. This is significantly higher than the AIE found in the control run. Although we can assume that this result is dependent on the prescribed supersaturation, the difference between this experiment and the control run indicates that the competition effect is crucial for understanding the low AIE found in this study. AIE and changes in effective radius and LWP for this sensitivity study are listed in Table 3 under experiment S_fixed.

4.2. Sensitivity to Critical Radius for Autoconversion

[38] A considerable sensitivity to variations in the critical radius for the onset of autoconversion was found to by *Rotstayn* [2000] and *Menon et al.* [2002]. In order to investigate this sensitivity in CAM-Oslo, we carried out two 1-year model runs with 4 months of spin-up assumed, one for PD conditions and one for PI conditions. In both runs we set the critical radius for the onset of autoconversion (r_{3lc}) to 7.5 μm.

[39] A very small reduction in the AIE of approximately 7% was found compared to the case of r_{3lc} = 15 μm. The reduction is assumed to be associated with a reduction in the anthropogenic change in LWP. However, the absolute value of LWP and therefore also the COD becomes smaller, possibly corresponding to a more sensitive environment for changes in cloud microphysical properties in terms of radiative effects, as will be discussed further in section 5. AIE and changes in effective radius and LWP for this experiment are listed in Table 3 under experiment R_{crit}7.5.

4.3. Sensitivity to Variations in the Hygroscopicity of Dust

[40] The sensitivity of the AIE to PI aerosol burdens was investigated by *Menon et al.* [2002] and found to be significant. In this study we have taken a slightly different approach, as we have carried out two sensitivity studies varying the hygroscopicity of dust. Both approaches lead to significant differences in PI concentrations of CCN. Many GCM studies of the AIE assume dust to be hydrophobic, hence the soluble mass fraction is assumed to be zero. However, some studies indicate that the soluble fraction of dust may in fact be significantly higher, depending on the mineralogy of the dust aerosols. As estimates of dust soluble fraction range from ∼0 [e.g., *Stier et al.*, 2005] to 0.13 [*Ghan et al.*, 2001], we chose to carry out our control run with an intermediate value for the soluble fraction for dust of 0.013. However, since estimates vary by orders of magnitude, we have performed two sensitivity tests, one for a soluble fraction of ∼0 and one for a soluble fraction of 0.13.

[41] We find that the AIE is highly sensitive to the hygroscopicity of mineral dust, as we find a decrease by a factor of two (−0.13 W/m^2) for a mineral dust soluble fraction of 0.13. For a soluble fraction of approximately zero, the AIE increases by approximately the same factor, resulting in an AIE of −0.72 W/m^2. AIE and changes in effective radius and LWP associated with this sensitivity test are given in Table 3 under experiment Min_hyg+ (soluble fraction of 0.13) and experiment Min_hyg− (Soluble fraction of ∼0).

5. Discussion and Comparison with Other Studies

[42] The aerosol indirect effect found in this study is significantly lower than that found in most other comparable studies (−1.1 W/m^2 to −1.5 W/m^2 [*Lohmann et al.*, 2000], −2.1 W/m^2 [*Rotstayn*, 1999], −1.55 W/m^2 to −4.36 W/m^2 [*Menon et al.*, 2002]). *Lohmann and Feichter* [2005] reported the estimated AIE from 10 different models to be ranging from approximately −1 W/m^2 to −3 W/m^2, but pointed out that inverse calculations starting from climate record data of oceanic and atmospheric warming suggest a smaller AIE within the range of 0 to −2 W/m^2. Compared to *Kristjánsson* [2002], our AIE is reduced by a factor of six, from −1.83 to −0.30 W/m^2. However, when the scheme used by *Kristjánsson* [2002] was implemented into NCAR CAM2.0 the AIE was reduced to −0.91 W/m^2 [*Storelvmo and Kristjánsson*, 2004]. This reduction was connected entirely to the change of model version. We believe this reduction to be due to changes in the amount of cloud liquid water and the cloud overlap assumption in the model. The

Table 3. Aerosol Indirect Effect and Changes in r_{eff} and LWP for the Control Run and Four Sensitivity Runs

	Indirect Effect, W/m^2	Change in Effective Radius, μm	Change in Liquid Water Path, g/m^2
Control	−0.30	−0.40	0.68
Min_hyg +	−0.13	−0.10	0.26
Min_hyg −	−0.72	−0.73	1.32
R_{crit} 7.5	−0.28	−0.39	0.60
S_fixed	−0.48	−0.59	1.54

globally averaged LWP is approximately 50% higher in NCAR CAM2.0 compared to the previous model version. As discussed by *Kiehl et al.* [2000] and *Ghan et al.* [1997], the SWCF associated with an optically thick cloud is relatively insensitive to changes in the optical depth. An environment with increased cloud LWP and hence liquid cloud optical depth would therefore be relatively insensitive to an increase in CCN. *Kiehl et al.* [2000] derived a proportionality between the AIE and cloud optical depth on the basis of equation (22.84) of *Seinfeld and Pandis* [1998]. This relationship is given in equation (5) for a cloud droplet asymmetry factor of 0.85. The expression "Normalized Forcing" is adopted from *Kiehl et al.* [2000], and corresponds to the right hand side of equation (5). The insensitivity to an increase in cloud optical depth in an already optically thick cloud is evident.

$$\Delta F_{indirect} \propto -\frac{\tau}{(\tau + 6.7)^2} \tag{5}$$

[43] Additionally, a maximum random (M/R) cloud overlap is assumed in NCAR CAM2.0 [*Collins*, 2001], while random cloud overlap was assumed in NCAR CCM3. M/R cloud overlap means that clouds in adjacent cloud layers are maximally overlapped, while cloud regions separated by one or more model layers are randomly overlapped. A M/R cloud overlap implies that cloud layers in the lower troposphere are more frequently shielded by higher cloud layers. The reflectivity of the cloud top is the dominating one in the radiative flux calculations, although lower cloud levels can have an influence if the top layer is optically thin. If the temperature at the cloud top is below freezing level, the IAE in the column will be negligible as we don't let the aerosols influence ice phase clouds. If the cloud top temperature is above freezing level the AIE will still be suppressed because of the rapid decrease in aerosol number concentration with height.

[44] In our current AIE scheme the aerosols are not allowed to influence the cloud fraction, as mentioned in section 2.1. Studies by *Koren et al.* [2005] and *Kaufman et al.* [2005] show that the aerosol effect on cloud cover can in some cases be substantial, and hence an important one in terms of radiative forcing. This is supported by equation (5), where increasing cloud optical thickness in a cloud free or optically thin fraction of the grid box corresponds to a strong negative cloud forcing, while adding a $\Delta\tau$ to an already optically thick fraction of the grid box has approximately no radiative effect. It should also be pointed out that this study does not account for all aspects of aerosol-cloud interaction.

[45] The small AIE can be attributed to several factors, the most important ones being the competition effect, the introduction of microphysical sinks for cloud droplet number, and a relatively high number of CCN in the PI case due to the slightly soluble mineral dust aerosols. The sensitivity to the first factor was tested in section 4.1. Our aerosol size distribution is designed in such a manner that the anthropogenic aerosol mass only contributes to the aerosol number concentration in the nucleation modes. The anthropogenic aerosol mass mixed internally with the background modes is simply added onto the preexisting aerosol particles. This leads to a growth of the aerosol particles, which in turn leads to a higher activated fraction. However, an increase in nucleation mode particles will contribute to the competition effect and decrease the maximum supersaturation, S_{max}. Hence the competition effect partially cancels the effect of larger aerosols in the internally mixed modes.

[46] In a model intercomparison presented by *Penner et al.* [2006], results from CAM-Oslo with diagnostic rather than prognostic treatment of cloud droplet number are presented. For a mineral dust soluble fraction of 0.13 and other parameters being similar to those of the control run, an AIE of -0.37 W/m^2 was found. This result illustrates the reduction in AIE that the inclusion of cloud droplet sinks leads to in the model. The cloud droplet sinks included in equation (4) are typically more efficient in a cloud with high CDNC (i.e., polluted clouds) than in clouds with low CDNC (i.e., clean clouds). Consequently, the inclusion of cloud droplet sinks reduces the difference in CDNC between a clean and a polluted cloud.

[47] Finally, it should be pointed out that the aerosol emissions applied in this study are different from the ones used by *Kristjánsson* [2002]. In this study, some isolated areas can actually have higher aerosol number concentration in the preindustrial run than under present-day conditions, as OC concentrations at NH high latitudes are higher in the PI case than in the PD case (see Figure 1c). This was not allowed to happen by *Kristjánsson* [2002].

6. Conclusion and Future Plans

[48] The aerosol indirect effect obtained in this study is significantly lower than most other estimates of the AIE. Reasons for this low number are discussed in the previous section.

[49] Four factors seem to be particularly important: (1) the increase of cloud water in the model version used in this study compared to previous NCAR GCM versions. (2) The transition to maximum $\neq$ random cloud overlap in this model version, while previous model versions assumed completely random overlap. (3) The implementation of a continuity equation for cloud droplets number with microphysical sinks of CDNC. (4) The introduction of a so-called competition effect, implying that a polluted cloud will correspond to lower maximum supersaturation compared to a relatively clean cloud.

[50] We consider these factors to all represent important steps toward a more realistic treatment of the interaction between aerosols and liquid clouds. However, we are not accounting for all aspects of aerosol-cloud interaction and the room for improvements is evident. Ideally, the cloud droplet number should be transported not only vertically but also horizontally.

[51] An important step toward complete consistency would be to develop a continuity equation also for aerosol number concentration. Additionally, it seems to be crucial to extend our AIE scheme in such a manner that aerosols are allowed to modify not only the cloud optical depth, but also cloud fraction. Observations on the dust mineralogy around the globe seem to be crucial in order to obtain accurate hygroscopicity estimates for use in GCM studies. However, even if such estimates were obtained, the uncertainty associated with PI aerosol burdens is still adding complexity

to quantifying the AIE. The indirect effect of aerosols on ice clouds is still a big challenge for the scientific community, but potentially very important. A treatment of aerosol-ice-cloud interactions in CAM-Oslo is under development and will be addressed in a later paper.

[52] **Acknowledgments.** The work presented in this paper has been supported by the Norwegian Research Council through the COMBINE project (grant 155968/S30), the AerOzClim project (grant 155974/720), and the RegClim project (grant 155975/S30). Furthermore, this work has received support of the Norwegian Research Council's program for Supercomputing through a grant of computer time. S. Ghan was supported by the U.S. Department of Energy Atmospheric Radiation Measurement Program and Atmospheric Science Program, which are part of the DOE Biological and Environmental Research Program. The Pacific Northwest National Laboratory is operated for the DOE by Battelle Memorial Institute under contract DE-AC06-76RLO 1830. Finally, we would like to thank one anonymous reviewer for comments that led to major improvements of the paper.

References

Abdul-Razzak, H., and S. Ghan (2000), A parameterization of aerosol activation: 2. Multiple aerosol type, *J. Geophys. Res.*, *105*, 6837–6844.

Abdul-Razzak, H., and S. J. Ghan (2002), A parameterization of aerosol activation: 3. Sectional representation, *J. Geophys. Res.*, *107*(D3), 4026, doi:10.1029/2001JD000483.

Abdul-Razzak, H., S. Ghan, and C. Rivera-Carpio (1998), A parameterization of aerosol activation: 1. Single aerosol type, *J. Geophys. Res.*, *103*, 6123–6131.

Albrecht, B. A. (1989), Aerosols, cloud microphysics, and fractional cloudiness, *Science*, *245*, 1227–1230.

Beheng, K. D. (1994), A parameterization of warm cloud microphysical conversion processes, *Atmos. Res.*, *33*, 193–206.

Charlson, R. J. (1988), Have the concentrations of tropospheric aerosol particles changed?, in *The Changing Atmosphere*, edited by F. S. Rowland and I. S. A. Isaksen, pp. 79–90, John Wiley, Hoboken, N. J.

Collins, W. D. (2001), Parameterization of generalized cloud overlap for radiative calculations in general circulation models, *J. Atmos. Sci.*, *58*, 3224–3242.

Ghan, S. J., L. R. Leung, R. C. Easter, and H. Abdul-Razzak (1997), Prediction of cloud droplet number in a general circulation model, *J. Geophys. Res.*, *102*, 21,777–21,794.

Ghan, S. J., G. Guzman, and H. Abdul-Razzak (1998), Competition between sea salt and sulfate particles as cloud condensation nuclei, *J. Atmos. Sci.*, *55*, 3340–3347.

Ghan, S. J., N. S. Laulainen, R. C. Easter, R. Wagener, S. Nemesure, E. G. Chapman, Y. Zhang, and L. R. Leung (2001), Evaluation of aerosol direct radiative forcing in MIRAGE, *J. Geophys. Res.*, *106*, 5295–5316.

Greenwald, T. J., G. L. Stephens, T. H. Vonder Haar, and D. L. Jackson (1993), A physical retrieval of cloud liquid water over the global oceans using special sensor microwave/imager (SSM/I) observations, *J. Geophys. Res.*, *98*, 18,471–18,488.

Han, Q., W. B. Rossow, and A. A. Lacis (1994), Near-global survey of effective droplet radii in liquid water clouds using ISCCP data, *J. Clim.*, *7*, 465–497.

Han, Q., W. B. Rossow, J. Chou, and R. M. Welch (1998), Global variations of column droplet concentration in low-level clouds, *Geophys. Res. Lett.*, *27*, 3221–3224.

Hansen, J., M. Sato, and R. Ruedy (1997), Radiative forcing and climate response, *J. Geophys. Res.*, *102*, 6831–6864.

Iversen, T., and Ø. Seland (2002), A scheme for process-tagged SO_4 and BC aerosols in NCAR CCM3: Validation and sensitivity to cloud processes, *J. Geophys. Res.*, *107*(D24), 4751, doi:10.1029/2001JD000885.

Kanakidou, M., et al. (2005), Organic aerosol and climate modelling: A review, *Atmos. Chem. Phys.*, *5*, 1053–1123.

Kaufman, Y. J., I. Koren, L. A. Remer, D. Rosenfeld, and Y. Rudich (2005), The effect of smoke, dust, and pollution aerosol on shallow cloud development over the Atlantic ocean, *Proc. Natl. Acad. Sci. U. S. A.*, *102*, 11,207–11,212.

Kiehl, J. T., T. L. Schneider, P. J. Rasch, and M. C. Barth (2000), Radiative forcing due to sulfate aerosols from simulations with the National Center for Atmospheric Research Community Climate Model, version 3, *J. Geophys. Res.*, *105*, 1441–1457.

Kirkevåg, A., and T. Iversen (2002), Global direct radiative forcing by process-parameterized aerosol optical properties, *J. Geophys. Res.*, *107*(D20), 4433, doi:10.1029/2001JD000886.

Kirkevåg, A., T. Iversen, Ø. Seland, and J. E. Kristjánsson (2005), Revised schemes for aerosol optical parameters and cloud condensation nuclei, *Inst. Rep. Ser. 128*, Dept. of Geosci. Univ. of Oslo, Norway.

Koren, I., Y. J. Kaufman, D. Rosenfeld, L. A. Remer, and Y. Rudich (2005), Aerosol invigoration and restructuring of Atlantic convective clouds, *Geophys. Res. Lett.*, *32*, L14828, doi:10.1029/2005GL023187.

Kristjánsson, J. E. (2002), Studies of the aerosol indirect effect from sulfate and black carbon aerosols, *J. Geophys. Res.*, *107*(D15), 4246, doi:10.1029/2001JD000887.

Lohmann, U., and J. Feichter (2005), Global indirect aerosol effects: A review, *Atmos. Chem. Phys.*, *5*, 715–737.

Lohmann, U., J. Feichter, C. C. Chuang, and J. E. Penner (1999), Predicting the number of cloud droplets in the ECHAM GCM, *J. Geophys. Res.*, *104*, 9169–9198.

Lohmann, U., J. Feichter, C. C. Chuang, and J. E. Penner (2000), Indirect effect of sulfate and carbonaceous aerosols: A mechanistic treatment, *J. Geophys. Res.*, *105*, 12,193–12,206.

Lohmann, U., K. Broekhuizen, R. Leaitch, N. Shantz, and J. Abbatt (2004), How efficient is cloud droplet formation of organic aerosols?, *Geophys. Res. Lett.*, *31*, L05108, doi:10.1029/2003GL018999.

Menon, S., A. D. Del Genio, D. Koch, and G. Tselioudis (2002), GCM simulations of the aerosol indirect effect: Sensitivity to cloud parameterization and aerosol burden, *J. Atmos. Sci.*, *59*, 692–713.

Penner, J. E., et al. (2001), Aerosols, their direct and indirect effects, in *Climate Change 2001: The Scientific Basis: Contribution of Working Group I to the Third Assessment Report of the Intergovernmental Panel on Climate Change*, edited by J. T. Houghton et al., chap. 5, pp. 289–348, Cambridge Univ. Press, New York.

Penner, J., J. Quaas, T. Storelvmo, T. Takemura, O. Boucher, H. Guo, A. Kirkevåg, J. E. Kristjánsson, and Ø. Seland (2006), Model intercomparison of the aerosol indirect effect, *Atmos. Chem. Phys.*, *6*, 3391–3405.

Rasch, P. J., and J. E. Kristjánsson (1998), A comparison of the CCM3 model climate using diagnosed and predicted condensate parameterizations, *J. Clim.*, *11*, 1587–1614.

Rosenfeld, D., R. Lahav, A. Khain, and M. Pinsky (2002), The role of sea spray in cleansing air pollution over ocean via cloud processes, *Science*, *297*, 1667–1670.

Rotstayn, L. D. (1999), Indirect forcing by anthropogenic aerosols: A global climate model calculation of the effective-radius and cloud-lifetime effects, *J. Geophys. Res.*, *104*, 9369–9380.

Rotstayn, L. D. (2000), On the "tuning" of autoconversion parameterizations in climate models, *J. Geophys. Res.*, *105*, 15,495–15,508.

Schultz, M., et al. (2006), Radiative forcing by aerosols as derived from the AeroCom present-day and pre-industrial simulations, *Atmos. Chem. Phys.*, *6*, 5225–5246.

Seinfeld, J. H., and S. N. Pandis (1998), *Atmospheric Chemistry and Physics: From Air Pollution to Climate Change*, 1326 pp., John Wiley, Hoboken, N. J.

Slingo, A. (1989), A GCM parameterization for the shortwave properties of water clouds, *J. Atmos. Sci.*, *46*, 1419–1427.

Stier, P., et al. (2005), The aerosol-climate model ECHAM5–HAM, *Atmos. Chem. Phys.*, *5*, 1125–1156.

Storelvmo, T., and J. E. Kristjánsson (2004), Studies of the aerosol indirect effect in NCAR CAM 2.0, in *Proceedings: 14th International Conference on Clouds and Precipitation*, vol. 1, pp. 239–242, World Meteorol. Org., Bologna, Italy, 18–23 Jul.

Storelvmo, T., J. E. Kristjánsson, G. Myhre, M. Johnsrud, and F. Stordal (2006), Combined observational and modeling based study of the aerosol indirect effect, *Atmos. Chem. Phys.*, *6*, 3583–3601.

Twomey, S. (1977), The influence of pollution on shortwave albedo of clouds, *J. Atmos. Sci.*, *34*, 1149–1152.

Weng, F., and N. C. Grody (1994), Retrieval of cloud liquid water using the special sensor microwave imager (SSM/I), *J. Geophys. Res.*, *99*, 25,535–25,551.

T. Iversen, A. Kirkevåg, J. E. Kristjánsson, Ø. Seland, and T. Storelvmo, Department of Geosciences, University of Oslo, P.O. Box 1022 Blindern, Oslo 0315, Norway. (truds@geo.uio.no)

S. J. Ghan, Pacific Northwest National Laboratory, 790 6th Street, ETB/2229/K9-24, Richland, WA 99354-1873, USA.